Journal of Hazardous Materials 416 (2021) 125860

Contents lists available at ScienceDirect

Journal of Hazardous Materials

journal homepage: www.elsevier.com/locate/jhazmat

Research Paper

Facile room temperature synthesis of ultra-small sized porous organic cages for fluorescent sensing of copper ion in aqueous solution

Cong Dai [a,b], Hai-Long Qian [c,d,e], Xiu-Ping Yan [c,d,e,*]

[a] College of Chemistry and Materials Science, Hengyang Normal University, Hengyang 421001, China
[b] Hunan Engineering Research Center for Monitoring and Treatment of Heavy Metals Pollution in the Upper Reaches of Xiangjiang River, Hengyang 421001, China
[c] State Key Laboratory of Food Science and Technology, Jiangnan University, Wuxi 214122, China
[d] Institute of Analytical Food Safety, School of Food Science and Technology, Jiangnan University, Wuxi 214122, China
[e] Key Laboratory of Synthetic and Biological Colloids, Ministry of Education, School of Chemical and Material Engineering, Jiangnan University, Wuxi 214122, China

ARTICLE INFO

Editor: Dr. C. LingXin

Keywords:
Facile preparation
Nano porous organic cages
Fluorescence sensing
Copper ion

ABSTRACT

Facile synthesis of nano porous organic cages with small size and good fluorescence property is highly desirable, but still challenging and scarce for their sensing applications. Here we report a rapid room-temperature recrystallization method for the preparation of nano porous organic cages with ultra-small size as a fluorescent probe for copper ion. The prepared nano porous organic cages gave the diameter of 2.49 ± 0.04 nm, and exhibited stable emission at 535 nm with absolute quantum yield of 0.68%. On the basis of the coordination interaction and charge transfer between the nano porous organic cages and copper ion, a simple fluorescent probe for copper ion in aqueous solution was developed. The developed method gave a calibration function of $QE = 0.4815\lg[Cu^{2+}] + 0.5847$ (where QE is the quenching efficiency; $[Cu^{2+}]$ in μM) ($R^2 = 0.9987$) in a concentration range of 0.1–2 μM, the limit of detection (3s) of 8 nM, and the relative standard deviation of 0.36% for 10 replicate determinations of 0.5 μM copper ion. The recoveries of spiked copper ion in tap water samples ranged from 96.8% to 103.0%. The proposed method possesses good sensitivity, selectivity and accuracy.

1. Introduction

Porous organic cages self-assembled from discrete imine-based molecule, as a new kind of porous materials, have received great attention recently (Tozawa et al., 2009; Holst et al., 2010; Mastalerz, 2018; Jones et al., 2011). Porous organic cages possess good chirality, and are soluble in solvents, such as dichloromethane. Owing to the window-to-window packing of cage molecules, porous organic cages have intrinsic and extrinsic porosity. Thus, porous organic cages have been applied in various fields (Bushell et al., 2013; Mitra et al., 2013; Chen et al., 2014; Kewley et al., 2015; Sun et al., 2015; Zhang et al., 2015, 2018; Hasell et al., 2016; Liu et al., 2016, 2019; Song et al., 2016; Miklitz et al., 2017; Yang et al., 2018; Lu et al., 2019; Wang et al., 2019b; Liang et al., 2020), such as gas adsorption and separation (Chen et al., 2014; Hasell et al., 2016; Miklitz et al., 2017; Liang et al., 2020; Wang et al., 2019b), chromatographic enantioseparation (Zhang et al., 2015; Kewley et al., 2015; Zhang et al., 2018), nanoparticle protecting (Sun et al., 2015; Yang et al., 2018; Lu et al., 2019) and hydrogen isotope separation (Liu et al., 2019). Moreover, the fluorescence emission of porous organic cages originating from benzene and imine fluorophore provides great potential for fluorescent sensing application. However, the application of porous organic cages in fluorescence sensing has not been reported so far.

The time-consuming crystalline growing method of homochiral CC3 (a kind of porous organic cages synthesized via [4 + 6] condensation of 1,3,5-triformylbenzene and homochiral cyclohexane-1,2-diamine) led to the formation of micrometer sized homochiral CC3 crystals, which is against the sensing application of porous organic cages (Tozawa et al., 2009). Racemic CC3 was also synthesized via homochiral CC3 solution mixing (Hasell et al., 2012). Fine size control of racemic CC3 from 50 nm to 1 μm was achieved by varying the mixing rate and temperature. In spite of no requirement of surfactants or templates, the preparation of nano racemic CC3 needs slow mixing at low temperature, even at −80 °C. Therefore, it is of high interest to develop a simple method to fabricate nano porous organic cages for broad potential applications in sensing.

Copper ion plays an important role in many fields, such as agriculture, chemical industry, and metabolic process (Stern et al., 2007; Fan

* Corresponding author at: State Key Laboratory of Food Science and Technology, Jiangnan University, Wuxi 214122, China.
E-mail address: xpyan@jiangnan.edu.cn (X.-P. Yan).

https://doi.org/10.1016/j.jhazmat.2021.125860
Received 20 January 2021; Received in revised form 6 April 2021; Accepted 7 April 2021
Available online 10 April 2021

et al., 2017, 2018; Wu et al., 2020). However, excessive copper ions are harmful for environment and biological system, which may lead to vomiting, Alzheimer's disease, and so on (Stern et al., 2007). Therefore, it is vital to develop a simple and sensitive method for the monitoring of copper ion in environmental water samples. Compared to traditional methods, such as atom emission spectrometry and mass spectrometry, inexpensive fluorescent sensing methods with high sensitivity and selectivity have attracted broad attention (Prodi et al., 2000). Fluorescence small molecular probes usually show difficulties in their poor water solubility for aqueous analysis (Sivaraman et al., 2018; Dai et al., 2015). Thus, various fluorescence nano probes have been developed to enhance the copper ion sensing efficiency in aqueous solution (Chen et al., 2017, 2019; Chabok et al., 2019; Lan et al., 2019; Qing et al., 2019; Yang et al., 2019; Zhang et al., 2019a, 2019b). For example, polyethylenimine-derived polymer dots were reported recently as fluorescence nano probe for copper ion and hypochlorite ion (Zhang et al., 2019a). However, complicated design, tedious preparation and modification, and generally large size (hundreds nanometer) of these probes are unfavorable for the fluorescence sensing of copper ion in aqueous solution.

In this work, we report a rapid room-temperature recrystallization method for the preparation of nano porous organic cages with ultra-small size as a fluorescent probe for copper ion. The proposed simple room-temperature recrystallization method gives the prepared nano porous organic cages with the diameter of 2.49 ± 0.04 nm as well as good fluorescence property for sensing application. The prepared nano porous organic cages show strong and selective affinity to copper ion, and was applied as a fluorescent probe for sensing of copper ion in aqueous solution with good sensitivity and selectivity.

2. Experimental section

2.1. Reagents

All reagents used are at least of analytical grade. 2,4,6-Triformylphloroglucinol (TP) was bought from Yanshen Technology Co., Ltd. (Jilin, China). (1R,2R)-cyclohexane-1,2-diamine (R,R-1,2-DACH), Na_2HPO_4, Na_2SO_4, $NaHCO_3$, NaAc, NaCl, KCl, $CaCl_2$, $CdCl_2$, $CoCl_2$, $CrCl_3$, $MgSO_4$, $MnCl_2$, $NiSO_4$, $PbCl_2$, $ZnSO_4$, $AlCl_3$, $FeCl_3$, and $ZrCl_4$ were obtained from Aladdin Co., Ltd. (Shanghai, China). Sodium diethyldithiocarbamate trihydrate (DDTC) was bought from Xianding Biotechnology Co., Ltd. (Shanghai, China). Ethanol (EtOH) was purchased from Concord Technology (Tianjin, China). Ultrapure water was bought from Hangzhou Wahaha Group Co. (Hangzhou, China).

2.2. Instrumentation and characterization

Fourier transform infrared (FTIR) spectra in KBr were recorded on an IRPrestige-21 spectrometer (Shimadzu, Japan). The transmission electron microscopy (TEM) image was collected on a Talos F200S transmission electron microscope (FEI, USA) with an accelerating voltage of 200 kV. N_2 adsorption-desorption experiments were performed on an ASAP 2460 micropore physisorption analyzer (Micromeritics, USA) at 77 K. Hydrodynamic size and zeta potential were determined on a Nano-ZS Zetasizer (Malvern, UK). X-ray photoelectron spectroscopy (XPS) analysis was conducted on an Escalab 250Xi spectrometer fitted with a monochromated Al Kα X-ray source (hν = 1486.6 eV), hybrid (magnetic/electrostatic) optics, and a multichannel plate and delay line detector (Thermo Fisher, UK). Mass spectra (MS) were acquired on a SolariX-70FT-MS (Bruker Daltonics, Germany). ^{1}H nuclear magnetic resonance spectra (^{1}H NMR) and ^{13}C nuclear magnetic resonance spectra (^{13}C NMR) were obtained on an Avance III HD 500 MHz spectrometer with tetramethyl silane (TMS) as an internal standard (Bruker, Switzerland). The absorption spectra were recorded on a UV-2501P spectrophotometer (Shimadzu, Japan). Fluorescence spectra were measured on a PTI QuantaMaster 8000 spectrofluorometer (Horiba, Canada). Absolute quantum yield was determined on a FLS980 spectrofluorometer (Edinburgh, UK).

2.3. Synthesis of porous organic cages (TP-CC3-R)

TP-CC3-R was synthesized according to Zhang et al. (2020). 42 mg of TP, 69 mg of R,R-1,2-DACH, and 200 μL of 1 M NaOH were dispersed in 5 mL of EtOH. The resulting mixture was then stirred at room temperature overnight. After EtOH was removed via vacuum distillation, the yellowish-brown powder of TP-CC3-R was obtained by washing with H_2O, centrifugation (10,000 rpm, 15 min), and further vacuum drying overnight. ^{1}H NMR (DMSO-D6): δ 9.7–11.8 (Ar–OH, 12H), 7.5–8.1 (HC=N, 12H), 3.0–3.3 (NCH, 12H), 2.1–1.6 (CH_2, 48H) ppm. ^{13}C NMR (DMSO-D6): δ 183.8 (HO–C in benzene ring, 12C), 155.5 (N=CH, 12 C), 106.0 (N=CH–C in benzene ring, 12C), 57.5 (N–CH, 12C), 34.8 and 25.2 (CH_2 in cyclohexane group, 24C) ppm. MS ($[M+H]^+$): Accurate mass calculated for $C_{72}H_{85}N_{12}O_{12}$: 1309.641. Found: 1309.643 for TP-CC3-R.

2.4. Synthesis of nano porous organic cages (nano TP-CC3-R)

6 mL of 7.5 mg/mL TP-CC3-R EtOH solution was mixed with 12 mL of H_2O rapidly. Yellowish-white precipitation was observed after 1-min recrystallization. The precipitation was collected by centrifugation (6000 rpm, 5 min), and then redispersed in 40 mL of H_2O. A small number of large nanoparticles were removed by centrifugation (6000 rpm, 5 min). Finally, the resulting yellowish-white supernatant solution containing 0.4 mg/mL of nano TP-CC3-R with ultra-small size was obtained.

2.5. Procedures for the optimization of fluorescence detection of copper ion

A certain amount of copper ion was added to 6 mL of 1 μg/mL nano TP-CC3-R solution. Fluorescence spectra were recorded to evaluate the effect of pH, incubation time, and copper ion concentration on fluorescence quenching. The quenching efficiency (*QE*) was calculated using the following Eq. (1).

$$QE = (F_0 - F_1)/F_0 \quad (1)$$

where F_0 and F_1 are the fluorescence intensities of the prepared nano TP-CC3-R before and after the incubation with copper ion.

2.6. Collection, pretreatment, and analysis of water samples

Tap water samples were collected locally and diluted 2 times with ultrapure water. After all samples were adjusted to pH 7.4 with 1 M NaOH, 15 μL of 0.4 mg/mL nano TP-CC3-R was mixed with 6 mL of sample solution. The fluorescence spectra were recorded after 3 h incubation.

3. Results and discussion

3.1. Synthesis and characterization of nano TP-CC3-R

Scheme 1 shows the developed room-temperature recrystallization method for the preparation of nano TP-CC3-R and the principle for fluorescence detection of copper ion in aqueous solution. To obtain nano TP-CC3-R, TP-CC3-R was first fabricated via stirring overnight at room temperature. Then, the nano TP-CC3-R was prepared by recrystallization in EtOH/H_2O (1/2, V/V) at room temperature.

TP-CC3-R was characterized by ^{1}H NMR, ^{13}C NMR and MS (Figs. S1–S3). The results show the successful synthesis of TP-CC3-R via the room temperature stirring method. The characteristic FTIR peaks of CH_2 at 2933 and 2857 cm^{-1}, the peak of C=N at 1603 cm^{-1}, and the peak of C=C at 1543 cm^{-1} for TP-CC3-R without recrystallization also indicate

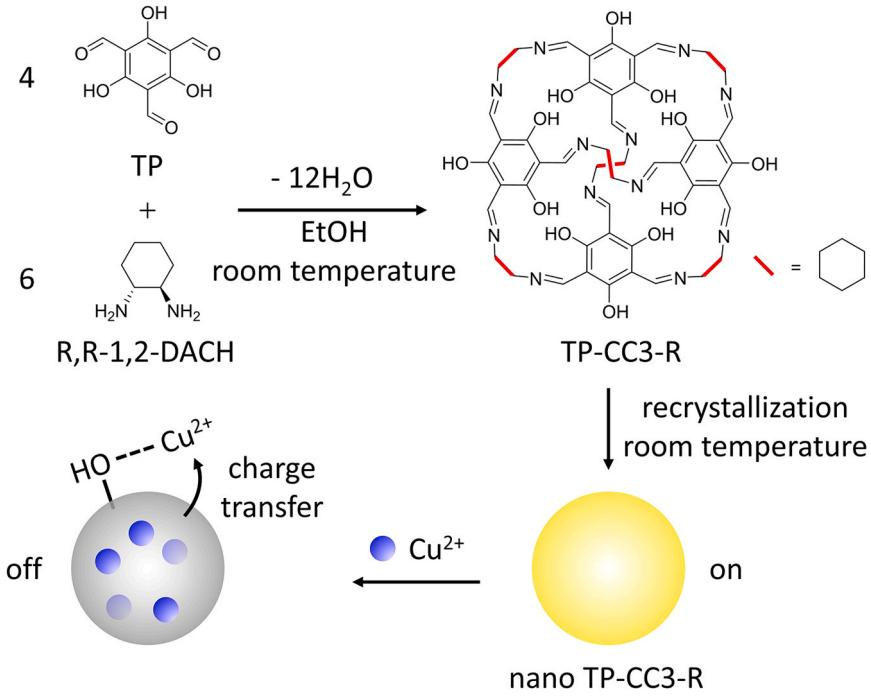

Scheme 1. Schematic illustration for the facile preparation of nano TP-CC3-R at room temperature and the mechanism for fluorescence sensing of copper ion in aqueous solution.

the successful fabrication of TP-CC3-R (Fig. 1A). The presence of the characteristic FTIR peaks of TP-CC3-R without recrystallization in nano TP-CC3-R demonstrates no obvious change of the structure of TP-CC3-R after recrystallization (Fig. 1A). The TEM image shows the nano TP-CC3-R with an ultra-small size of 2.49 ± 0.04 nm and a lattice spacing of 0.18 nm (Fig. 1B). The pore size of 1.69 nm shows the porosity of nano TP-CC3-R while the Brunauer–Emmett–Teller surface area of 23.8 m^2/g indicates only intrinsic porosity but no formally connected pores in the nano TP-CC3-R, which is similar to CC1 (a kind of porous organic cages synthesized with ethylene diamine and 1,3,5-triformylbenzene) (Figs. S4, S5) (Tozawa et al., 2009).

To obtain the ultra-small sized nano TP-CC3-R, the synthetic parameters was optimized. No yellowish-white precipitation was obtained in EtOH/H_2O (1/1, V/V). The hydrodynamic diameter increased as the decrease of EtOH/H_2O (V/V) from 1/2 to 1/4 (Table S1). In addition, no obvious difference of hydrodynamic diameter was observed when the recrystallization time increased from 1 min to 5 min (Table S1). Thus, EtOH/H_2O (1/2, V/V) and 1-min recrystallization were used to synthesize nano TP-CC3-R. The recrystallization gave much smaller hydrodynamic diameter of nano TP-CC3-R (278.7 ± 11.7 nm) than that of the TP-CC3-R without recrystallization (735.3 ± 23.0 nm), indicating the significant effect of recrystallization on the size of nano TP-CC3-R (Fig. 1C). The zeta potential of nano TP-CC3-R in pH 7.4 was 24.5 ± 0.8 mV, which is close to that of TP-CC3-R without recrystallization (24.4 ± 2.2 mV). Moreover, the zeta potential of nano TP-CC3-R increased as pH decreased from 12 to 3 owing to the protonation of nitrogen and oxygen atoms in nano TP-CC3-R (Fig. S6).

The absorption peaks of TP-CC3-R without recrystallization at 244, 287, 328, and 356 nm exhibited great difference from TP, indicating the successful synthesis of TP-CC3-R via stirring overnight at room temperature (Fig. 2A). The prepared nano TP-CC3-R gave the absorption peaks at 245, 296, 336, and 360 nm (Fig. 2A). A slight red-shift of each absorption peak was observed in comparison to the absorption of TP-CC3-R without recrystallization because of J-type molecule assembly during the recrystallization at room temperature (Vybornyi et al., 2013).

The TP-CC3-R without recrystallization gave an emission at 525 nm with an apparent red-shift compared to the emission of TP at 508 nm (Fig. S7). The apparent red-shift was caused by reabsorption due to the aggregation of fluorophore in TP-CC3-R (Dai et al., 2015; Mizusawa et al., 2010). After molecule assembly during the recrystallization, the nano TP-CC3-R exhibited an emission at 535 nm under the excitation at 360 nm, also showing a red-shift in comparison to the emission of TP-CC3-R without recrystallization due to the J-type assembly (Fig. 2B) (Vybornyi et al., 2013). Confining to the reabsorption and J-type assembly, the absolute quantum yield of the nano TP-CC3-R at pH 7.4 is 0.68%. The nano TP-CC3-R also shows good stability in the pH range of 7–12, revealing good pH stability of nano TP-CC3-R (Fig. 2C). But because of the protonation of nitrogen and oxygen atoms in nano TP-CC3-R, the fluorescence of nano TP-CC3-R decrease along with the decrease of pH from 7 to 3 (Fig. 2C). Moreover, the prepared nano TP-CC3-R possesses good long-term colloidal stability for at least 8 days (Fig. 2D). The above results indicate the successful synthesis of nano TP-CC3-R with ultra-small size, good fluorescence property and stability.

3.2. Interaction between nano TP-CC3-R and copper ion

The nano TP-CC3-R incubated with copper ion was characterized by FTIR. The unchanged characteristic peaks of nano TP-CC3-R at 2933, 2857, 1603, and 1543 cm^{-1} show no structural change of nano TP-CC3-R after the incubation with copper ion (Fig. 1A). Besides, the appearance of the peaks of Cu–O at 632 and 477 cm^{-1} reveals the formation of Cu–O coordination bond between copper ion and the oxygen atom in nano TP-CC3-R (Fig. 1A) (Nakamoto, 2009).

The XPS spectra of nano TP-CC3-R were also been recorded to investigate the interaction between nano TP-CC3-R and copper ion. The XPS peak of N 1s was still located at 399.7 eV after the incubation with copper ion, indicating no formation of Cu-N coordination interaction (Fig. S8). The deprotonated O 1s in nano TP-CC3-R incubated with copper ion gave higher binding energy at 530.5 eV in comparison to that in nano TP-CC3-R (530.4 eV) (Fig. 3A and B). Moreover, the relative content of deprotonated oxygen atom increased after the incubation (Fig. 3A and B). Both the higher binding energy and the increased content indicate the charge transfer from deprotonated oxygen atom in

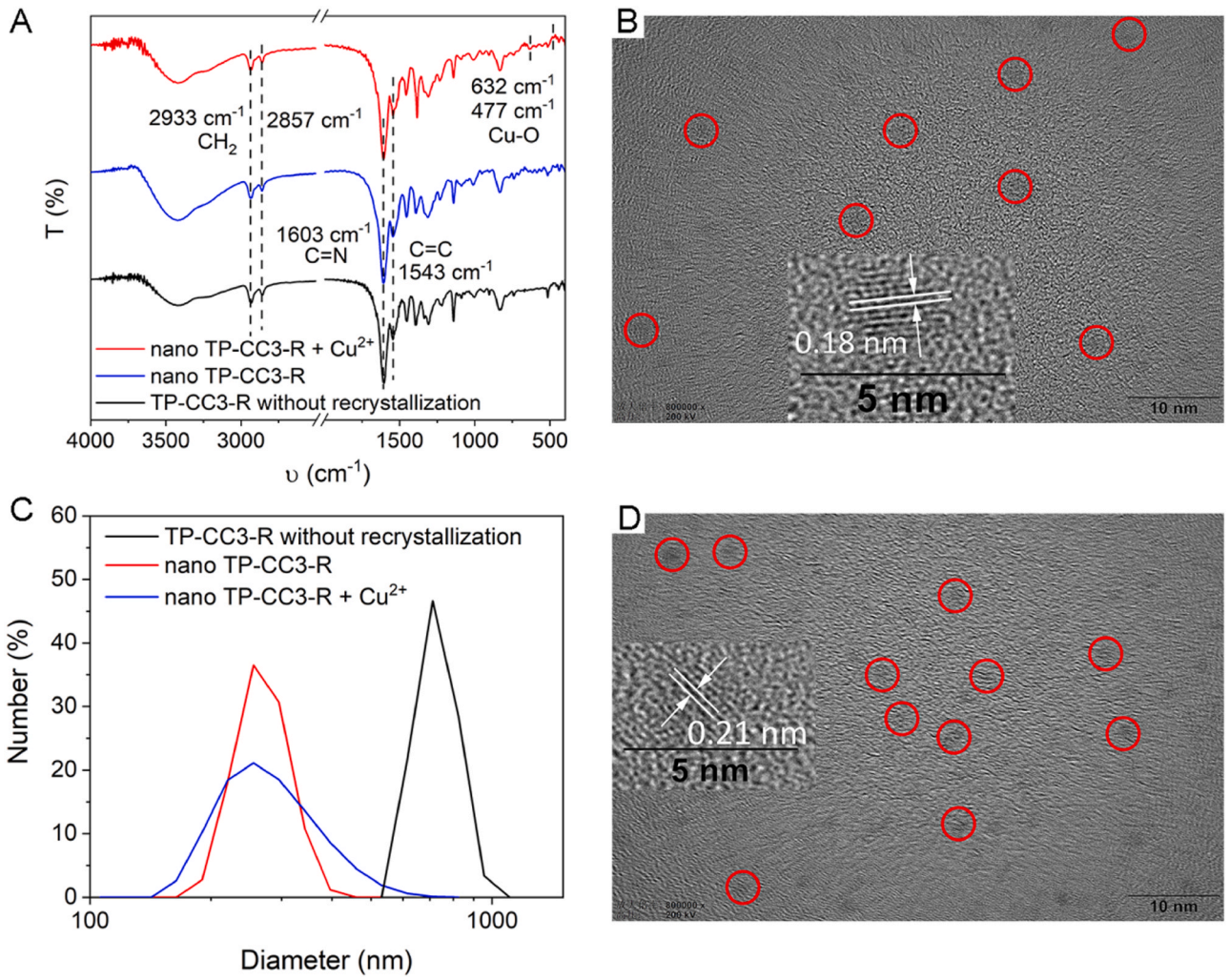

Fig. 1. (A) FTIR spectra of TP-CC3-R without recrystallization (black), the as-prepared nano TP-CC3-R alone (blue) or incubated with copper ion (red). (B) TEM image and lattice fringes (inset) of nano TP-CC3-R. (C) Hydrodynamic diameter of TP-CC3-R without recrystallization (black), the as-prepared nano TP-CC3-R alone (red) or incubated with copper ion (blue). (D) TEM image and lattice fringes (inset) of nano TP-CC3-R incubated with copper ion. (For interpretation of the references to colour in this figure legend, the reader is referred to the web version of this article.)

nano TP-CC3-R to copper ion after the formation of Cu–O bond (Wang et al., 2019a; Yoshida, 1980). In addition, the decrease of the binding energy and the relative content of protonated oxygen atom in nano TP-CC3-R also shows the transformation of oxygen atom from protonation to deprotonation after the incubation (Fig. 3A and B) (Wang et al., 2019a; Yoshida, 1980). The XPS peaks of Cu $2p_{3/2}$ at 934.2 eV, Cu $2p_{1/2}$ at 954.0 eV, and the satellite shake-up peaks at 943.8 and 963.8 eV in nano TP-CC3-R incubated with copper ion, also reveal the presence of copper ion and the formation of Cu–O bond (Fig. S9) (Wang et al., 2019a). In contrast, no XPS peak of copper ion was recorded before the incubation with copper ion (Fig. S9).

After the interaction with copper ion, the diameter of nano TP-CC3-R (2.51 ± 0.08 nm) is comparable to that of nano TP-CC3-R before the incubation (2.49 ± 0.04 nm), showing no obvious influence of copper ion to the diameter of nano TP-CC3-R (Fig. 1D). However, interaction with copper ion made the lattice spacing of nano TP-CC3-R slightly increase from 0.18 to 0.21 nm, revealing an amorphous transformation due to the entry of copper ion in the interior of nano TP-CC3-R (Fig. 1B cf. 1D). In addition, the average hydrodynamic diameter of nano TP-CC3-R incubated with copper ion (267.8 ± 9.1 nm) is almost the same as nano TP-CC3-R (Fig. 1C). However, a wider size distribution of the hydrodynamic diameter was observed due to the transformation of partial nano TP-CC3-R to smaller or larger nanoparticles resulting from the dissociation and reassembly of nano TP-CC3-R after the interaction with copper ion (Fig. 1C). Furthermore, the zeta potential of nano TP-CC3-R increased significantly with the concentration of copper ion owing to the charge transfer from nano TP-CC3-R to the empty orbital of copper ion, suggesting the coordination interaction between copper ion and nano TP-CC3-R (Fig. 3C).

All the absorption peaks of nano TP-CC3-R increased and the absorption at 336 and 360 nm blue-shifted slightly with the increase of the concentration of copper ion (Fig. 3D). Both the increase and blue-shift were relevant to the increase of energy band gap of $\pi \rightarrow \pi^*$ transition of nano TP-CC3-R due to the charge transfer from nano TP-CC3-R to copper ion (Nguyen and Scheschkewitz, 2005). The UV–vis spectra of TP-CC3-R without recrystallization incubated with copper ion also verified the increase and blue-shift of absorption caused by Cu–O coordination bond (Fig. S10). The above results indicate the Cu–O coordination interaction between the prepared nano TP-CC3-R and copper ion in aqueous solution.

3.3. Fluorescence detection of copper ion

Because of the charge transfer from nano TP-CC3-R to the empty orbital of copper ion after the formation of Cu–O coordination bond, the non-radiative transition of excited electron increased while the energy

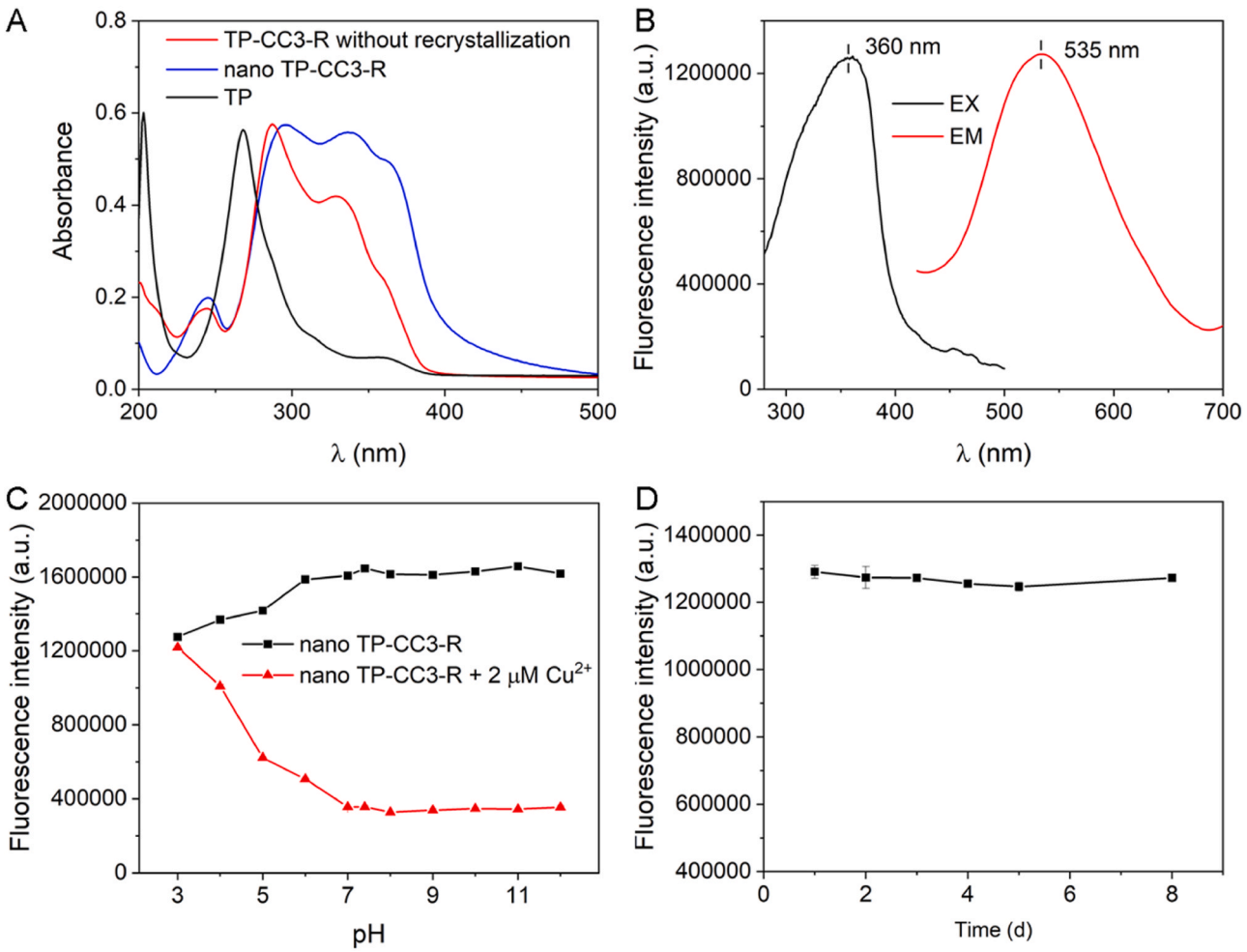

Fig. 2. (A) UV–vis absorption spectra of TP (black), TP-CC3-R without recrystallization (red), and nano TP-CC3-R (blue). (B) Fluorescence excitation (black) and emission (red) spectra of nano TP-CC3-R. (C) Effect of pH on the fluorescence intensity of nano TP-CC3-R before (black) and after (red) the incubation with copper ion. (D) Long-term colloidal stability of nano TP-CC3-R. (For interpretation of the references to colour in this figure legend, the reader is referred to the web version of this article.)

band gap of π→π* transition increased. As a result, the emission at 535 nm of the nano TP-CC3-R decreased gradually in conjugation with a slight blue-shift, depending on the concentration of copper ion (Fig. 4A). The fluorescence photos also indicate the decrease of the green fluorescence of nano TP-CC3-R as the concentration of copper ion increased (Fig. S11). The *QE* increased with the concentration of copper ion (Fig. 4B). In addition, the *QE* gradually increased as incubation time before 3 h incubation (Fig. S12). The obvious fluorescence quenching offers the great potential of nano TP-CC3-R as a turn-off fluorescence probe for the detection of copper ion in aqueous solution.

The effect of pH on the fluorescence of nano TP-CC3-R with 2 μM copper ion in aqueous solution was tested. The fluorescence intensity decreased and the *QE* increased notably as pH increased from 3 to 7 because of the increased coordination ability of deprotonated nano TP-CC3-R to copper ion at higher pH (Figs. 2C and 4C). Besides, in spite of the transformation of partial copper ion to copper hydroxide in the pH range of 7–12, the fluorescence intensity and the *QE* remained almost unchanged (Figs. 2C and 4C). The results indicate no obvious effect of copper hydroxide formation on the strong coordination affinity of nano TP-CC3-R to copper ion. In addition, the effect of pH on the adsorption ability of nano TP-CC3-R to copper ion was also tested (Fig. S13). The adsorption efficiency increased significantly as pH increased from 3 to 7, convincing the increased coordination ability of deprotonated nano TP-CC3-R to copper ion. The adsorption ability increased slightly as pH increased from 7 to 12, which is coinciding to the almost constant fluorescence *QE*. Thus, the following experiments were performed at pH 7.4 with highest *QE*.

We also examined the change of *QE* of nano TP-CC3-R with the concentration of copper ion in aqueous solution. Considering the sensitivity of detection, nano TP-CC3-R was incubated with copper ion for 3 h to obtain the maximal *QE*. The *QE* linearly increased with the denary logarithm of the copper ion concentration ($lg[Cu^{2+}]$) in a concentration range of 0.1–2 μM, with a calibration function of $QE = 0.4815lg[Cu^{2+}] + 0.5847$ ($[Cu^{2+}]$ in μM, $R^2 = 0.9987$) (Fig. 4B). The limit of detection (3*s*) was 8 nM, which is comparable to or better than those obtained by other fluorescence probes for copper ion in aqueous solution (Table S2). The relative standard deviation for 10 replicate detections of 0.5 μM copper ion was 0.36%, showing good precision of the proposed method for copper ion detection. Considering the rapidity of detection, copper ion sensing based on nano TP-CC3-R was also achieved with 5-min incubation. Much smaller *QE* was observed than that of 3 h incubation. The *QE* linearly increased with $lg[Cu^{2+}]$ in a concentration range of 0.1–1000 μM, with a calibration function of $QE = 0.1420lg[Cu^{2+}] + 0.2128$ ($[Cu^{2+}]$ in μM, $R^2 = 0.9953$) (Fig. S14). Compared to 3 h incubation, the short incubation time led to wider linear range but lower sensitivity.

To explore the effect of recrystallization on detection performance, the TP-CC3-R before recrystallization was also applied to copper ion sensing with 5-min incubation. The calibration function was $QE = 0.2110lg[Cu^{2+}] + 0.1095$ ($[Cu^{2+}]$ in μM, $R^2 = 0.9858$) in a

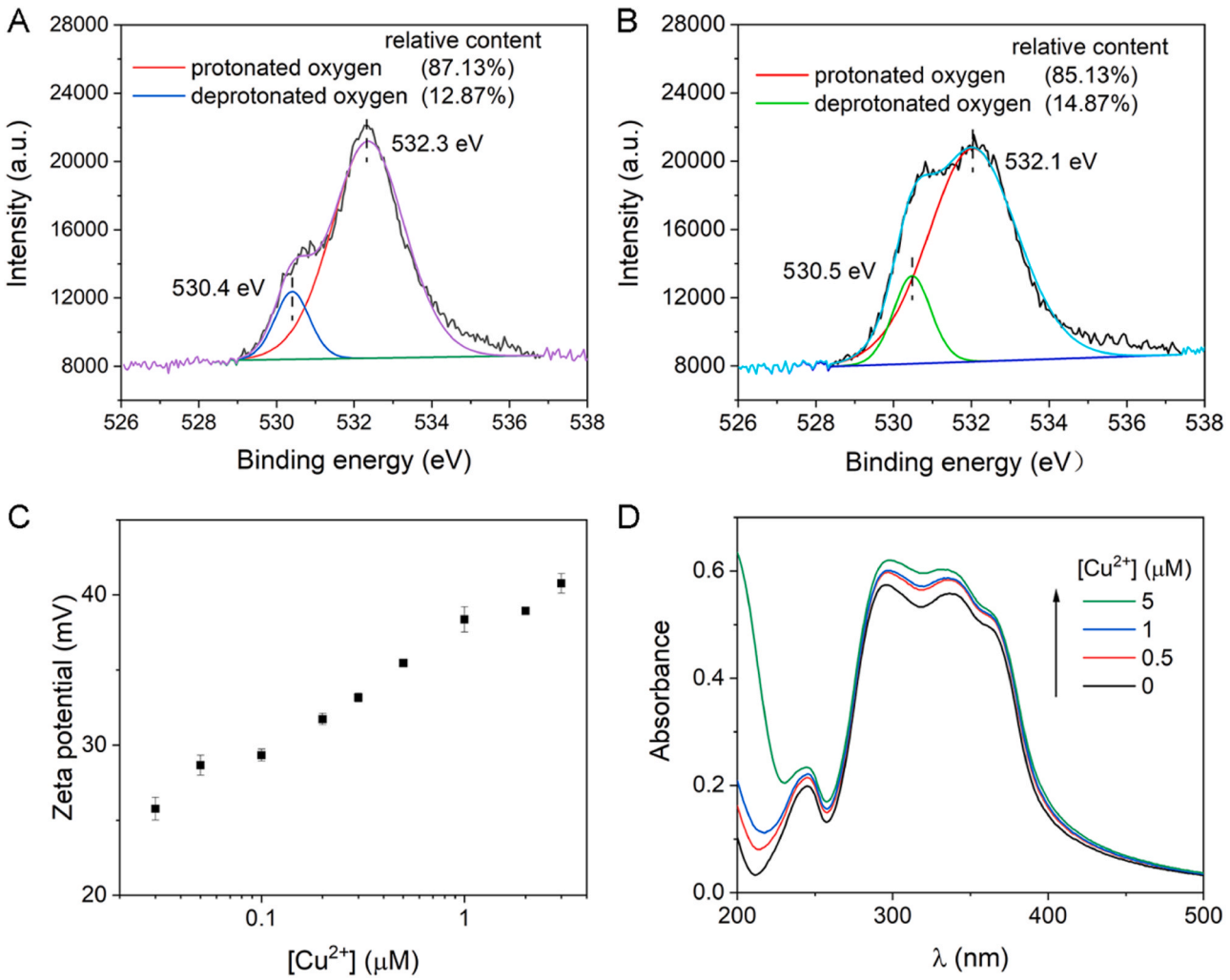

Fig. 3. XPS O 1s spectra of nano TP-CC3-R before (A) and after (B) the incubation with copper ion. Effect of copper ion concentration on zeta potential (C) and UV–vis spectra (D) of nano TP-CC3-R. (For interpretation of the references to colour in this figure, the reader is referred to the web version of this article.)

concentration range of 0.1–10 μM (Fig. S15). The linear range was much narrower and the correlation coefficient was worse than that of copper ion sensing based on the prepared nano TP-CC3-R. Moreover, the TP-CC3-R before recrystallization had strong precipitation tendency in aqueous solution owing to its large hydrodynamic diameter (735.3 ± 23.0 nm), hindering the accurate determination of fluorescence.

To evaluate the selectivity of the nano TP-CC3-R for the fluorescence sensing of copper ion in aqueous solution, the effect of coexisting ions on the *QE* of nano TP-CC3-R in the presence of 0.5 μM copper ion was examined. For comparison, the *QE* in the presence of coexisting ions was then normalized to that only in 0.5 μM copper ion. No obvious disturbance to the detection was observed, even in the presence of 10 times higher concentration of HPO_4^{2-}, SO_4^{2-}, HCO_3^-, Ac^-, Cl^-, K^+, Ca^{2+}, Cd^{2+}, Co^{2+}, Cr^{3+}, Mg^{2+}, Hg^{2+}, Mn^{2+}, Ni^{2+}, Pb^{2+}, and Zn^{2+} due to the weak competition coordination ability of these ions for the Cu–O coordination bond between nano TP-CC3-R and copper ion (Fig. 4D). Al^{3+}, Fe^{3+}, and Zr^{4+} have a little higher ability to quench fluorescence than the aforementioned coexisting ions, but they at 0.5 μM level still exhibited no obvious influence on the fluorescence of nano TP-CC3-R (Fig. S16). The tolerance concentration of Al^{3+}, Fe^{3+}, and Zr^{4+} was up to 0.5, 1, and 1 μM, respectively, which was enough for the copper ion detection in domestic water sample (Fig. 4D) (WHO, 2006). Besides, nano TP-CC3-R had much higher adsorption efficiency for Cu^{2+} (57.3%) than Co^{2+} (22.6%), Ni^{2+} (17.5%), Zn^{2+} (1.9%), Al^{3+} (24.9%), Fe^{3+} (1.7%), and Zr^{4+} (9.5%) (Table S3). The high adsorption efficiency for Cu^{2+} may account for the high selectivity of nano TP-CC3-R for copper ion sensing.

To show the practical utility of the nano TP-CC3-R, we applied it to detect copper ion in tap water samples. The recoveries of spiked copper ion in these samples ranged from 96.8% to 103.0%, indicating no significant interferences in the detection of copper ion in tap water samples (Table 1). The concentrations of copper ion in tap water determined by the proposed method are in good agreement with those measured by a DDTC (copper reagent) spectrophotometric method (Table 1). The above results reveal good selectivity, sensitivity, and accuracy of the proposed method for the detection of copper ion in tap water samples.

4. Conclusion

In summary, we have reported a facile room-temperature recrystallization method for fabricating ultra-small sized nano TP-CC3-R with good fluorescence property and stability for sensitive and selective sensing of copper ion in aqueous solution. On the basis of the coordination interacting between nano TP-CC3-R and copper ion, we have also proposed a nano TP-CC3-R based fluorescence probe for copper ion and successfully applied to the determination of copper ion in real water samples with good selectivity, sensitivity, and accuracy, highlighting the great potential of nano porous organic cages in sensing.

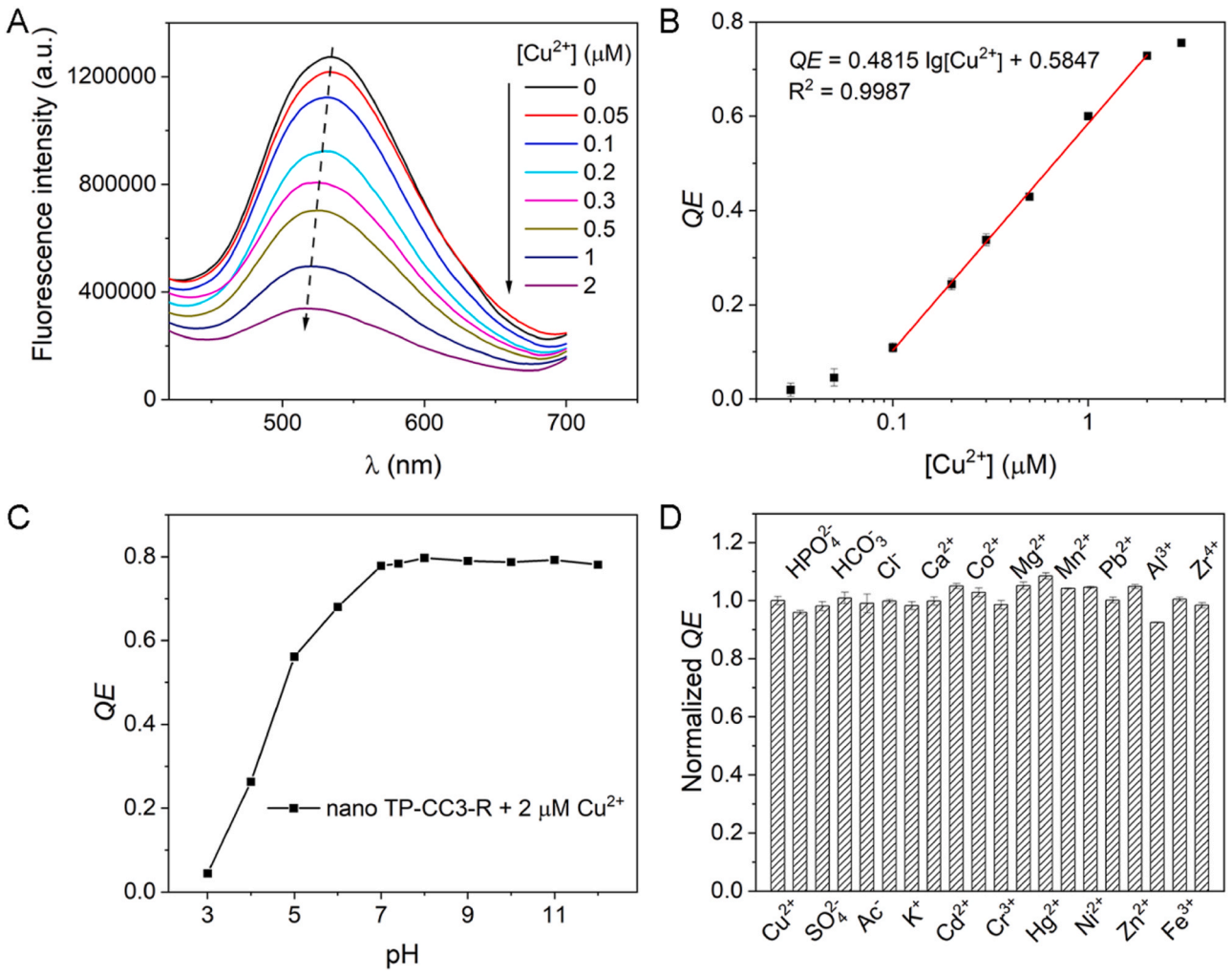

Fig. 4. (A) Copper ion concentration dependent fluorescence spectra of nano TP-CC3-R ([nano TP-CC3-R], 1 μg/mL; pH, 7.4; incubation time, 3 h). (B) Plot of the *QE* of nano TP-CC3-R as a function of the copper ion concentration ([nano TP-CC3-R], 1 μg/mL; pH, 7.4; incubation time, 3 h). (C) Effect of pH on the *QE* of nano TP-CC3-R incubated with copper ion ([nano TP-CC3-R], 1 μg/mL; incubation time, 3 h). (D) Normalized *QE* for 0.5 μM Cu^{2+} without or with various coexisting ions (0.5 μM Al^{3+}, 1 μM Fe^{3+}, 1 μM Zr^{4+}, 5 μM for others). ([nano TP-CC3-R], 1 μg/mL; pH, 7.4; incubation time, 3 h).

Table 1
Analytical results (Mean ± *s*, *n* = 3) for the determination of Cu^{2+} in tap water samples.

Samples	Concentration determined (μM)		Recovery (%)[a]
	The developed method	DDTC spectrophotometric method	
Tap water 1	0.731 ± 0.003	0.746 ± 0.002	99.0 ± 1.0
Tap water 2	0.700 ± 0.009	0.716 ± 0.002	96.8 ± 0.5
Tap water 3	0.756 ± 0.007	0.803 ± 0.008	103.0 ± 0.7

[a] spiked Cu^{2+}, 1 μM.

CRediT authorship contribution statement

Cong Dai: Methodology, Validation, Formal analysis, Investigation, Writing - original draft, Funding acquisition. **Hai-Long Qian:** Investigation. **Xiu-Ping Yan:** Writing - review & editing, Funding acquisition.

Declaration of Competing Interest

The authors declare that they have no known competing financial interests or personal relationships that could have appeared to influence the work reported in this paper.

Acknowledgments

This work was supported by the Youth Program of Nature Science Foundation of Hunan Province (2020JJ5008), the Scientific Research Fund of Hunan Provincial Education Department (20C0298), the Science Foundation of Hengyang Normal University (18D09), the National First-Class Discipline Program of Food Science and Technology (No. JUFSTR20180301), and the Program of "Collaborative Innovation Center of Food Safety and Quality Control in Jiangsu Province".

Appendix A. Supporting information

Supplementary data associated with this article can be found in the online version at doi:10.1016/j.jhazmat.2021.125860.

References

Bushell, A.F., Budd, P.M., Attfield, M.P., Jones, J.T.A., Hasell, T., Cooper, A.I., Bernardo, P., Bazzarelli, F., Clarizia, G., Jansen, J.C., 2013. Nanoporous organic polymer/cage composite membranes. Angew. Chem. Int. Ed. 52, 1253–1256. https://doi.org/10.1002/anie.201206339.

Chabok, A., Shamsipur, M., Yeganeh-Faal, A., Molaabasi, F., Molaei, K., Sarparast, M., 2019. A highly selective semiconducting polymer dots-based "off–on" fluorescent nanoprobe for iron, copper and histidine detection and imaging in living cells. Talanta 194, 752–762. https://doi.org/10.1016/j.talanta.2018.10.072.

Chen, J., Chen, H., Wang, T., Li, J., Wang, J., Lu, X., 2019. Copper ion fluorescent probe based on Zr-MOFs composite material. Anal. Chem. 91, 4331–4336. https://doi.org/10.1021/acs.analchem.8b03924.

Chen, L., Reiss, P.S., Chong, S.Y., Holden, D., Jelfs, K.E., Hasell, T., Little, M.A., Kewley, A., Briggs, M.E., Stephenson, A., Thomas, K.M., Armstrong, J.A., Bell, J., Busto, J., Noel, R., Liu, J., Strachan, D.M., Thallapally, P.K., Cooper, A.I., 2014. Separation of rare gases and chiral molecules by selective binding in porous organic cages. Nat. Mater. 13, 954–960. https://doi.org/10.1038/nmat4035.

Chen, L.F., Tian, X.K., Yang, C., Li, Y., Zhou, Z.X., Wang, Y.X., Xiang, F., 2017. Highly selective and sensitive determination of copper ion based on a visual fluorescence method. Sens. Actuators B Chem. 240, 66–75. https://doi.org/10.1016/j.snb.2016.08.155.

Dai, C., Yang, C.-X., Yan, X.-P., 2015. Ratiometric fluorescent detection of phosphate in aqueous solution based on near infrared fluorescent silver nanoclusters/metal–organic shell composite. Anal. Chem. 87, 11455–11459. https://doi.org/10.1021/acs.analchem.5b03086.

Fan, M., Hu, J., Cao, R., Xiong, K., Wei, X., 2017. Modeling and prediction of copper removal from aqueous solutions by nZVI/rGO magnetic nanocomposites using ANN-GA and ANN-PSO. Sci. Rep. 7, 18040. https://doi.org/10.1038/s41598-017-18223-y.

Fan, M., Hu, J., Cao, R., Ruan, W., Wei, X., 2018. A review on experimental design for pollutants removal in water treatment with the aid of artificial intelligence. Chemosphere 200, 330–343. https://doi.org/10.1016/j.chemosphere.2018.02.111.

Hasell, T., Chong, S.Y., Jelfs, K.E., Adams, D.J., Cooper, A.I., 2012. Porous organic cage nanocrystals by solution mixing. J. Am. Chem. Soc. 134, 588–598. https://doi.org/10.1021/ja209156v.

Hasell, T., Miklitz, M., Stephenson, A., Little, M.A., Chong, S.Y., Clowes, R., Chen, L., Holden, D., Tribello, G.A., Jelfs, K.E., Cooper, A.I., 2016. Porous organic cages for sulfur hexafluoride separation. J. Am. Chem. Soc. 138, 1653–1659. https://doi.org/10.1021/jacs.5b11797.

Holst, J.R., Trewin, A., Cooper, A.I., 2010. Porous organic molecules. Nat. Chem. 2, 915–920. https://doi.org/10.1038/nchem.873.

Jones, J.T., Hasell, T., Wu, X., Bacsa, J., Jelfs, K.E., Schmidtmann, M., Chong, S.Y., Adams, D.J., Trewin, A., Schiffman, F., Cora, F., Slater, B., Steiner, A., Day, G.M., Cooper, A.I., 2011. Modular and predictable assembly of porous organic molecular crystals. Nature 474, 367–371. https://doi.org/10.1038/nature10125.

Kewley, A., Stephenson, A., Chen, L., Briggs, M.E., Hasell, T., Cooper, A.I., 2015. Porous organic cages for gas chromatography separations. Chem. Mater. 27, 3207–3210. https://doi.org/10.1021/acs.chemmater.5b01112.

Lan, M., Zhao, S., Wu, S., Wei, X., Fu, Y., Wu, J., Wang, P., Zhang, W., 2019. Optically tunable fluorescent carbon nanoparticles and their application in fluorometric sensing of copper ions. Nano Res. 12, 2576–2583. https://doi.org/10.1007/s12274-019-2489-2.

Liang, J., Nuhnen, A., Millan, S., Breitzke, H., Gvilava, V., Buntkowsky, G., Janiak, C., 2020. Encapsulation of a porous organic cage into the pores of a metal-organic framework for enhanced CO_2 separation. Angew. Chem. Int. Ed. 59, 6068–6073. https://doi.org/10.1002/anie.201916002.

Liu, M., Chen, L., Lewis, S., Chong, S.Y., Little, M.A., Hasell, T., Aldous, I.M., Brown, C. M., Smith, M.W., Morrison, C.A., Hardwick, L.J., Cooper, A.I., 2016. Three-dimensional protonic conductivity in porous organic cage solids. Nat. Commun. 7, 12750. https://doi.org/10.1038/ncomms12750.

Liu, M., Zhang, L., Little, M.A., Kapil, V., Ceriotti, M., Yang, S., Ding, L., Holden, D.L., Balderas-Xicohtencatl, R., He, D., Clowes, R., Chong, S.Y., Schutz, G., Chen, L., Hirscher, M., Cooper, A.I., 2019. Barely porous organic cages for hydrogen isotope separation. Science 366, 613–620. https://doi.org/10.1126/science.aax7427.

Lu, Z., Lu, X., Zhong, Y., Hu, Y., Li, G., Zhang, R., 2019. Carbon dot-decorated porous organic cage as fluorescent sensor for rapid discrimination of nitrophenol isomers and chiral alcohols. Anal. Chim. Acta 1050, 146–153. https://doi.org/10.1016/j.aca.2018.11.006.

Mastalerz, M., 2018. Porous shape-persistent organic cage compounds of different size, geometry, and function. Acc. Chem. Res. 51, 2411–2422. https://doi.org/10.1021/acs.accounts.8b00298.

Miklitz, M., Jiang, S., Clowes, R., Briggs, M.E., Cooper, A.I., Jelfs, K.E., 2017. Computational screening of porous organic molecules for xenon/krypton separation. J. Phys. Chem. C 121, 15211–15222. https://doi.org/10.1021/acs.jpcc.7b03848.

Mitra, T., Jelfs, K.E., Schmidtmann, M., Ahmed, A., Chong, S.Y., Adams, D.J., Cooper, A. I., 2013. Molecular shape sorting using molecular organic cages. Nat. Chem. 5, 276–281. https://doi.org/10.1038/nchem.1550.

Mizusawa, K., Ishida, Y., Takaoka, Y., Miyagawa, M., Tsukiji, S., Hamachi, I., 2010. Disassembly-driven turn-on fluorescent nanoprobes for selective protein detection. J. Am. Chem. Soc. 132, 7291–7293. https://doi.org/10.1021/ja101879g.

Nakamoto, K., 2009. Infrared and Raman Spectra of Inorganic and Coordination Compounds, 6th ed. John Wiley & Sons, New Jersey.

Nguyen, T.L., Scheschkewitz, D., 2005. Activation of a Si"Si bond by η1-coordination to a transition metal. J. Am. Chem. Soc. 127, 10174–10175. https://doi.org/10.1021/ja052593p.

Prodi, L., Bolletta, F., Montalti, M., Zaccheroni, N., 2000. Luminescent chemosensors for transition metal ions. Coord. Chem. Rev. 205, 59–83. https://doi.org/10.1016/s0010-8545(00)00242-3.

Qing, T., Zhang, K., Qing, Z., Wang, X., Long, C., Zhang, P., Hu, H., Feng, B., 2019. Recent progress in copper nanocluster-based fluorescent probing: a review. Microchim. Acta 186, 670. https://doi.org/10.1007/s00604-019-3747-4.

Sivaraman, G., Iniya, M., Anand, T., Kotla, N.G., Sunnapu, O., Singaravadivel, S., Gulyani, A., Chellappa, D., 2018. Chemically diverse small molecule fluorescent chemosensors for copper ion. Coord. Chem. Rev. 357, 50–104. https://doi.org/10.1016/j.ccr.2017.11.020.

Song, Q., Jiang, S., Hasell, T., Liu, M., Sun, S., Cheetham, A.K., Sivaniah, E., Cooper, A.I., 2016. Porous organic cage thin films and molecular-sieving membranes. Adv. Mater. 28, 2629–2637. https://doi.org/10.1002/adma.201505688.

Stern, B.R., Solioz, M., Krewski, D., Aggett, P., Aw, T.C., Baker, S., Crump, K., Dourson, M., Haber, L., Hertzberg, R., Keen, C., Meek, B., Rudenko, L., Schoeny, R., Slob, W., Starr, T., 2007. Copper and human health: biochemistry, genetics, and strategies for modeling dose-response relationships. J. Toxicol. Environ. Health B Crit. Rev. 10, 157–222. https://doi.org/10.1080/10937400600755911.

Sun, J.K., Zhan, W.W., Akita, T., Xu, Q., 2015. Toward homogenization of heterogeneous metal nanoparticle catalysts with enhanced catalytic performance: soluble porous organic cage as a stabilizer and homogenizer. J. Am. Chem. Soc. 137, 7063–7066. https://doi.org/10.1021/jacs.5b04029.

Tozawa, T., Jones, J.T.A., Swamy, S.I., Jiang, S., Adams, D.J., Shakespeare, S., Clowes, R., Bradshaw, D., Hasell, T., Chong, S.Y., Tang, C., Thompson, S., Parker, J., Trewin, A., Bacsa, J., Slawin, A.M.Z., Steiner, A., Cooper, A.I., 2009. Porous organic cages. Nat. Mater. 8, 973–978. https://doi.org/10.1038/nmat2545.

Vybornyi, M., Rudnev, A.V., Langenegger, S.M., Wandlowski, T., Calzaferri, G., Häner, R., 2013. Formation of two-dimensional supramolecular polymers by amphiphilic pyrene oligomers. Angew. Chem. Int. Ed. 52, 11488–11493. https://doi.org/10.1002/anie.201307029.

Wang, J., Du, R., Liu, W., Yao, L., Ding, F., Zou, P., Wang, Y., Wang, X., Zhao, Q., Rao, H., 2019a. Colorimetric and fluorometric dual-signal determination of dopamine by the use of Cu-Mn-O microcrystals and C-dots. Sens. Actuators B Chem. 290, 125–132. https://doi.org/10.1016/j.snb.2019.03.107.

Wang, Z., Sikdar, N., Wang, S.-Q., Li, X., Yu, M., Bu, X.-H., Chang, Z., Zou, X., Chen, Y., Cheng, P., Yu, K., Zaworotko, M.J., Zhang, Z., 2019b. Soft porous crystal based upon organic cages that exhibit guest-induced breathing and selective gas separation. J. Am. Chem. Soc. 141, 9408–9414. https://doi.org/10.1021/jacs.9b04319.

WHO, 2006. Guidelines for Drinking-Water Quality, Recommendations, 3rd ed. World Health Organization, Geneva.

Wu, X., Hu, J., Qi, J., Hou, Y., Wei, X., 2020. Graphene-supported ordered mesoporous composites used for environmental remediation: a review. Sep. Purif. Technol. 239, 116511 https://doi.org/10.1016/j.seppur.2020.116511.

Yang, X., Sun, J.-K., Kitta, M., Pang, H., Xu, Q., 2018. Encapsulating highly catalytically active metal nanoclusters inside porous organic cages. Nat. Catal. 1, 214–220. https://doi.org/10.1038/s41929-018-0030-8.

Yang, Y.Z., Xiao, N., Cen, Y.Y., Chen, J.R., Liu, S.G., Shi, Y., Fan, Y.Z., Li, N.B., Luo, H.Q., 2019. Dual-emission ratiometric nanoprobe for visual detection of Cu(II) and intracellular fluorescence imaging. Spectrochim. Acta Part A Mol. Biomol. Spectrosc. 223, 117300 https://doi.org/10.1016/j.saa.2019.117300.

Yoshida, T., 1980. An X-ray photoelectron spectroscopic study of several hydroxy azo compounds. Bull. Chem. Soc. Jpn. 53, 498–501. https://doi.org/10.1246/bcsj.53.498.

Zhang, H., Dong, X., Wang, J., Guan, R., Cao, D., Chen, Q., 2019a. Fluorescence emission of polyethylenimine-derived polymer dots and its application to detect copper and hypochlorite ions. ACS Appl. Mater. Interfaces 11, 32489–32499. https://doi.org/10.1021/acsami.9b09545.

Zhang, J.H., Xie, S.M., Chen, L., Wang, B.J., He, P.G., Yuan, L.M., 2015. Homochiral porous organic cage with high selectivity for the separation of racemates in gas chromatography. Anal. Chem. 87, 7817–7824. https://doi.org/10.1021/acs.analchem.5b01512.

Zhang, J.H., Zhu, P.J., Xie, S.M., Zi, M., Yuan, L.M., 2018. Homochiral porous organic cage used as stationary phase for open tubular capillary electrochromatography. Anal. Chim. Acta 999, 169–175. https://doi.org/10.1016/j.aca.2017.11.021.

Zhang, L., Liang, R., Hang, C., Wang, H., Sun, L., Xu, L., Liu, D., Zhang, Z., Zhang, X., Chang, F., Zhao, S., Huang, W., 2020. A facile solution-phase synthetic approach for constructing phenol-based porous organic cages and covalent organic frameworks. Green Chem. 22, 2498–2504. https://doi.org/10.1039/c9gc04033a.

Zhang, W.J., Liu, S.G., Han, L., Luo, H.Q., Li, N.B., 2019b. A ratiometric fluorescent and colorimetric dual-signal sensing platform based on N-doped carbon dots for selective and sensitive detection of copper(II) and pyrophosphate ion. Sens. Actuators B Chem. 283, 215–221. https://doi.org/10.1016/j.snb.2018.12.012.